Electronic Supplementary Material (ESI) for ChemComm.

Supporting Information

Reversible Stimulus-Responsive Cu(I) Iodide Pyridine Coordination Polymer

Pilar Amo-Ochoa,* Khaled Hassanein, Carlos J. Gómez-García, Samia Benmansour, Josefina Perles, Oscar Castillo, José I. Martínez, Pilar Ocón and Félix Zamora*

Materials and Methods

2-amino-5-nitropyridine (ANP), CuI, and solvents were purchased from standard chemical suppliers and used as received. IR spectra were recorded on a PerkinElmer 100 spectrophotometer using a universal ATR sampling accessory and on a Bruker FT-IR Vector 22 model in the range 4000-400 cm^{-1} in KBr pellets. Elemental analyses were carried out by the microanalytical service of the Autónoma University of Madrid.

Powder X-ray diffraction were collected for polycrystalline samples filled into 0.5 mm (**1a**) and 0.7 mm (**1**) glass capillaries that were mounted and aligned on a X'Pert PRO θ/2θ PANalytical diffractometer with primary monochromator and detector with fast X'Celerator (or a Empyrean PANalytical diffractometer, for **1**) using Cu Kα radiation (λ = 1.54177 Å). The samples have been analysed with scanning θ/2θ.

Direct current (DC) electrical conductivity measurements were performed on different single crystals with carbon paint at 300 K and two contacts. The contacts were made with wolframium wires (25 μm diameter). The samples were measured at 300 K applying an electrical current with voltages form +10 to -10 V. The measurements were performed in the compounds along the crystallographic *a* axis. The thermal dependence of the DC electrical conductivity was measured with the four (or two, depending on the size of the crystals) contacts method on several (at least four) single crystals in the temperature range 2-300 K. The contacts were made with Pt wires (25 μm diameter) using graphite paste. The samples were measured in a Quantum Design PPMS-9 equipment connected to an external voltage source (Keithley model 2400 source-meter) and amperometer (Keithley model 6514 electrometer). All the conductivity quoted values have been measured in the voltage range where the crystals are Ohmic conductors. The cooling and warming rates were

0.5 and 1 K/min. The results were similar for all the measured crystals of each compound.

A device was built with a pellet of **1** electrically contacted with two copper wires (Figure S11). Electrical characterization of this pellet of **1** was done at room temperature by Electrochemical Impedance Spectroscopy (EIS) measurements. The samples were exposed to HAcO vapour at different times and the total pellet resistance (R) was obtained from the intercept of the arc (at the low frequency end) on the Z′ axis. The conductivity σ in S cm^{-1} was calculated from Z' value by using Eq. (1), where "*l*" is the pellet thickness in cm, "*R*" is the resistance in Ω and "*A*" is the electrode area in cm^2. The calculated conductivities of the samples are presented in Table S2.

$$\sigma = \frac{l}{R \cdot A} \qquad (1)$$

Electrochemical Impedance Spectroscopy data were collected at 298 K using an Autolab electrochemical system II PGSTAT30 (Ecochemie, The Netherlands) impedance analyser over the frequency range from 1 Hz to 1 MHz with an applied voltage of 0.01 V. The two-probe method was used in all the measurements. AC measurements through path and in line were performed to determine the conductivity parameters. The electrode samples were pressed pellets of thickness ranging between 1 and 2 mm. A powder sample (20 mg) was pressed by applying about 6 Tons/m^2 to form disks into a pellet with an area about 0.13-0.16 cm^2. The electrical contact between the sample and the symmetric stainless steel disk electrodes was made by applying pressure, about 10 Tons/m^2, with a conductivity cell configuration SS/**1**/SS, where SS refers to stainless steel and **1** refers to the solid pellet of compound **1**. Conductive carbon paint was used in order to connect compound **1** with the electric wire contact; in this case no pressure was applied.

The samples were exposed to acetic acid vapour for different times (15, 20, 45 min. and 24 h in order to ensure vapour saturation). The samples were introduced in a small close box containing pure HAcO. The samples never were in contact with liquid HAcO. After some time, they were left in the air in order to remove the acetic acid. Each impedance measurement was made three times, and different pellets were tested in order to corroborate the reproducibility of the measurements. The Z' values were obtained by fitting the depressed semi-circle with the real axis of the low frequency range using the ZView 3.1 (Scribner Association) Software.

The total impedance spectra can be fitted by an equivalent circuit such as bulk resistance and constant phase element (for bulk capacitance) in parallel with constant phase element (for interfacial capacitance) in series. Table S2 shows the different AC conductivity values for the compound **1**. The conductivity value changes dramatically from values approximately up to 10^{-11} Scm^{-1} to 10^{-6} Scm^{-1} at 298 K for pristine sample of compound **1** and saturated HAcO sample, respectively.

Single crystals of compounds **1** and **1a** were mounted on glass fibres or MiTeGen sample holders, using a viscous hydrocarbon oil to coat the crystals. Single crystal X-ray diffraction data were collected at 296 K on a Bruker Kappa Apex II (**1a**) and transferred directly to the cold nitrogen stream for data collection at 200 and 298 K on a Supernova diffractometer ($\mathbf{1^{LT}}$ and $\mathbf{1^{RT}}$, respectively). In all cases the diffractometers were equipped with a graphite-monochromated Mo Kα radiation (λ = 0.71073 Å).

Calculations were performed using the WINGX crystallographic software package for compounds $\mathbf{1^{LT}}$ and $\mathbf{1^{RT}}$.[1] For compound **1a** the software package SHELXTL was used for space group determination, structure solution, and refinement.[2] For compound **1** the program CrysAlisPro, Oxford Diffraction Ltd[3] was used for unit cell

determinations and data reduction. The structures were solved by direct methods, completed with difference Fourier syntheses, and refined by full-matrix least-squares on F^2 including all reflections (SHELXL97).[4] All non-hydrogen atoms were refined anisotropically. CCDC 1046598-1046600 contain the supplementary crystallographic data for this paper. Table S1 displays the crystallographic data and the structure refinement details.

Density Functional Theory (DFT)-based calculations by using the efficient plane-wave code QUANTUM ESPRESSO.[5] In this atomistic simulation package the Kohn-Sham equations are solved using a periodic supercell geometry. The ion-electron interaction is modelled by ultra-soft pseudopotentials,[6] and exchange-correlation (XC) effects are treated by the generalized-gradient-approximation (GGA) of Perdew, Burke, and Ernzerhof (PBE).[7] The one-electron wave-functions are expanded in a basis of plane-waves with energy cut-offs of 400 and 500 eV for the kinetic energy and for the electronic density, respectively, which have been adjusted to achieve sufficient accuracy in the total energy. The Brillouin zones of the different bulk-systems were sampled by using a **k**-space of $\Delta\mathbf{k} \leq 0.01 Å^{-1}$.[8]

Synthesis of $[Cu(C_5H_5N_3O_2)I]_n$, 1. CuI (50 mg, 0.26 mmol) and ANP (36 mg, 0.26 mmol) were dissolved in 12 mL acetonitrile. The resulting yellow solution was stirred for 2 h at 25 ºC. The final yellow solution was filtered off and left for crystallization at 25 ºC. After a week, yellow crystals, suitable for X-ray diffraction, were filtered, washed with water, acetonitrile and diethyl ether, and dried in air (38 mg, 44 % yield based on Cu). Anal. Calcd (found) for $C_5H_5CuN_3O_2I$: C, 18.22 (18.05); H, 1.53 (1.63); N, 12.75 (12.80). IR selected data (KBr, cm^{-1}): 3452 (m), 3326 (m), 1626 (s), 1603 (m), 1571 (m), 1335 (s), 1290 (s), 827 (m), 759 (w). The purity of the sample was confirmed by X-ray power diffraction (Figure S13).

Synthesis of {$[Cu(C_5H_5N_3O_2)I]_n$, 1a. CuI (50 mg, 0.26 mmol) and ANP (36 mg, 0.26 mmol) were stirred in 12 mL of acetonitrile-water (2:1) for 10 min at 25 ºC. The resulting yellow solution was sealed in a 23 mL Teflon-lined steel autoclave, heated at 160 ºC for 4 days, and finally cooled to 30 ºC at a rate of 5 ºC/h. Red crystals, suitable for X-ray diffraction, were filtered, washed with water, acetonitrile and

diethyl ether and air-dried (28 mg, 33 % yield based on Cu). Anal. Calcd. (found) for $C_5H_5CuN_3O_2I$: C, 18.22 (17.95); H, 1.53 (1.69); N, 12.75 (12.37). IR selected data (KBr, cm^{-1}): 3452 (m), 3326 (m), 1626 (s), 1603 (m), 1571 (m), 1335 (s), 1290 (s), 827 (m), 759 (w). The purity of the sample was confirmed by X-ray powder diffraction (Figure S15).

Theoretical Calculations. In order to rationalize the electronic conductivity experimental results, we have carried out a set of First-principles Density-functional-theory (DFT)-based calculations (further details in Figure S8). For the theoretical simulations, we have used the structures obtained by X-ray diffraction. For all the polymers, the residual forces acting on each atom in all the calculations were below 0.1 eV/Å, which is low enough to guarantee perfectly converged and realistic results for such complex systems from a theoretical point of view. This noticeably good geometrical transferability between the experimental configurations and our theoretical implementation has already provided successful results for other similar CPs.[9]

Additionally, to check the possible influence in the electronic conduction process of the hydrogen bonds stabilizing the whole bulk-crystal structure we have also performed electronic structure calculations of the isolated monodimensional polymeric chains for all the compounds. This strategy will permit the exclusion of the contribution of the hydrogen bonds formed between ligands within the electronic structure calculation. The result of these calculations reveals that the electronic structure of the isolated chains does not show any significant variation with respect to the electronic structure of the bulks, except for a slight electronic gap-opening below 5% of their corresponding bulk value. These findings corroborate that the hydrogen bonds between neighbouring ligands do not contribute to the electronic conduction.

Table S1. Crystallographic Data and Structure Refinement Details.

Compound	**1^{LT}**	**1^{RT}**	**1a**
Empirical formula	C_5H_5Cu IN_3O_2	C_5H_5Cu IN_3O_2	C_5H_5Cu IN_3O_2
Formula weight	329.56	329.56	329.56
λ (Å)	0.71073	0.71073	0.71073
T (K)	200(2)	298(2)	296(2)
Crystal system	monoclinic	monoclinic	monoclinic
Space group	*Pn*	$P2_1/n$	$P2_1/c$
a (Å)	4.1982(1)	4.2284(1)	4.0708(1)
b (Å)	14.3433(3)	14.3638(7)	7.5386 (2)
c (Å)	13.6017(3)	13.6840(5)	28.2779(7)
α (º)	90	90	90
β (°)	94.707(2)	95.241(3)	90.880(1)
γ (º)	90	90	90
V (Å^3)	816.28(3)	827.64(5)	867.69(4)
Z	4	4	4
ρ_{calcd} (g cm^{-3})	2.682	2.645	2.523
μ (mm^{-1})	6.417	6.329	6.036
Reflections collected	16183	3768	12161
Unique data/parameters	2861/233	1418/129	1560/109
Rint	0.0579	0.0294	0.0242
Goodness of fit (S)[a]	0.956	1.244	1.121
R_1[b]/wR_2[c] [I>2σ(I)]	0.221/0.0472	0.0482/0.0943	0.0201/0.0365
R_1[b]/wR_2[c] [all data]	0.0234/0.0479	0.0593/0.1005	0.0268/0.0395

[a] $S = [\sum w(F_0^2 - F_c^2)^2 / (N_{obs} - N_{param})]^{1/2}$

[b] $R_1 = \sum||F_0|-|F_c|| / \sum|F_0|$

[c] $wR_2 = [\sum w(F_0^2 - F_c^2)^2 / \sum wF_0^2]^{1/2}$; $w = 1/[\sigma^2(F_0^2) + (aP)^2 + bP]$ where $P = (\max(F_0^2,0) + 2Fc^2)/3$ with a = 0.0203 (**1^{LT}**), 0.0234 (**1^{RT}**), 0.0099 (**1a**), and b = 0.4030 (**1^{LT}**), 4.3558 (**1^{RT}**), 1.4616 (**1a**).

Table S2. AC conductivity values of compound **1** at room temperature and different exposition times to HAcO or $CHCl_3$ (vapour).

$HAcO_{(vapour)}$ time	σ_{298K} (Scm^{-1})	Time in the air	σ_{298K} (Scm^{-1})
0 min	$\sim 10^{-11}$		
15 min	2.2×10^{-7}		
20 min	9.6×10^{-7}		
45 min	2.2×10^{-6}	60 min	$\sim 10^{-11}$
24 h	2.5×10^{-6}	30 min	4.5×10^{-10}
$CHCl_{3(vapour)}$ time	σ_{298K} (Scm^{-1})		
24 h	3.59×10^{-10}		

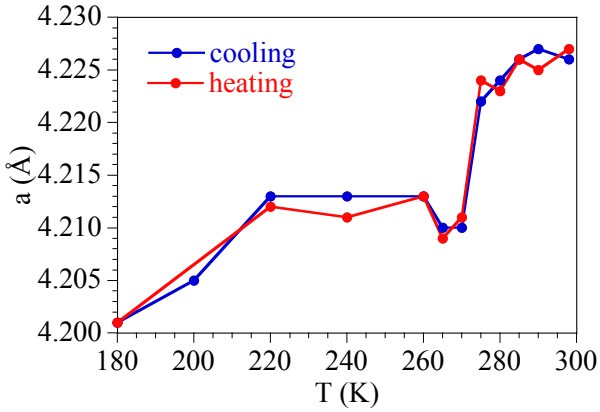

Figure S1. Thermal variation of the *a* unit cell parameter for compound **1**.

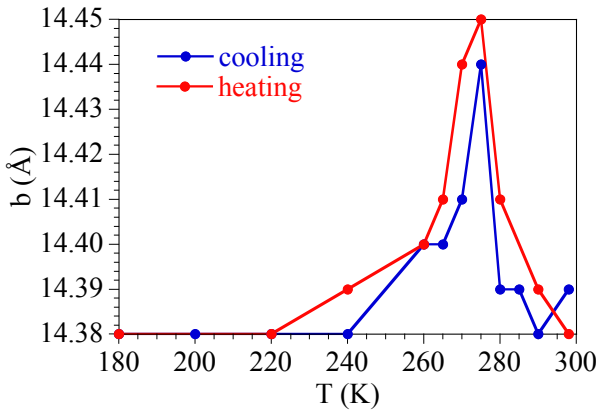

Figure S2. Thermal variation of the *b* unit cell parameter for compound **1**

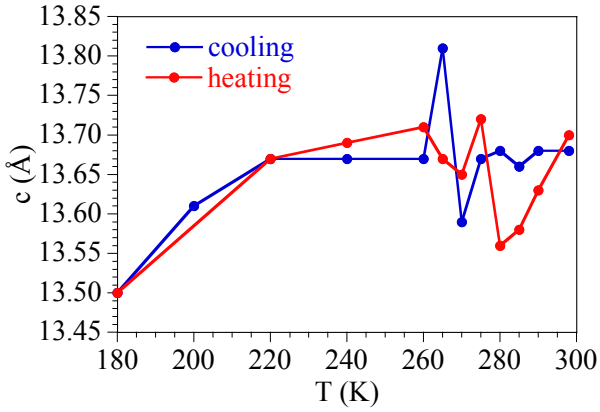

Figure S3. Thermal variation of the *c* unit cell parameter for compound **1**.

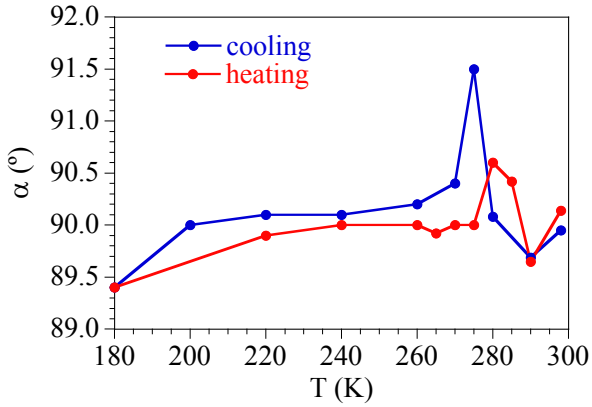

Figure S4. Thermal variation of the α unit cell parameter for compound **1**.

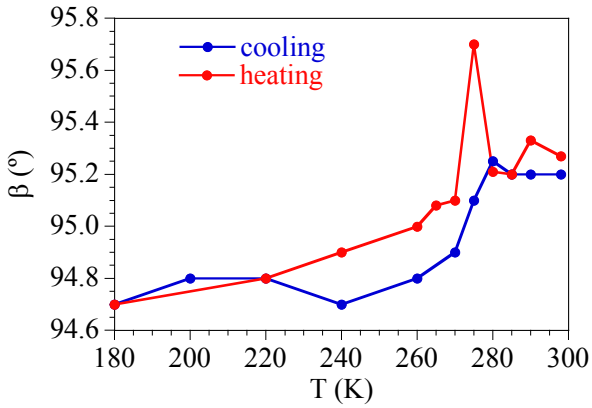

Figure S5. Thermal variation of the β unit cell parameter for compound **1**.

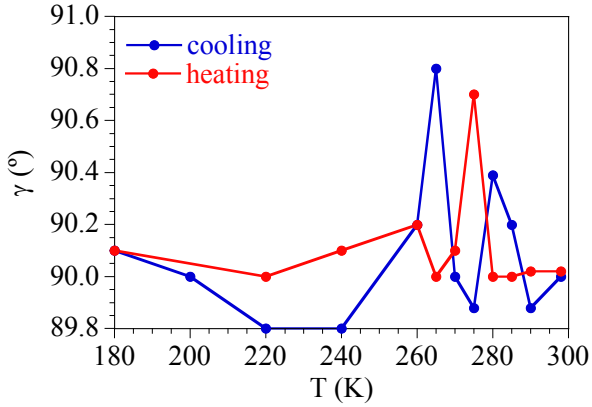

Figure S6. Thermal variation of the γ unit cell parameter for compound **1**.

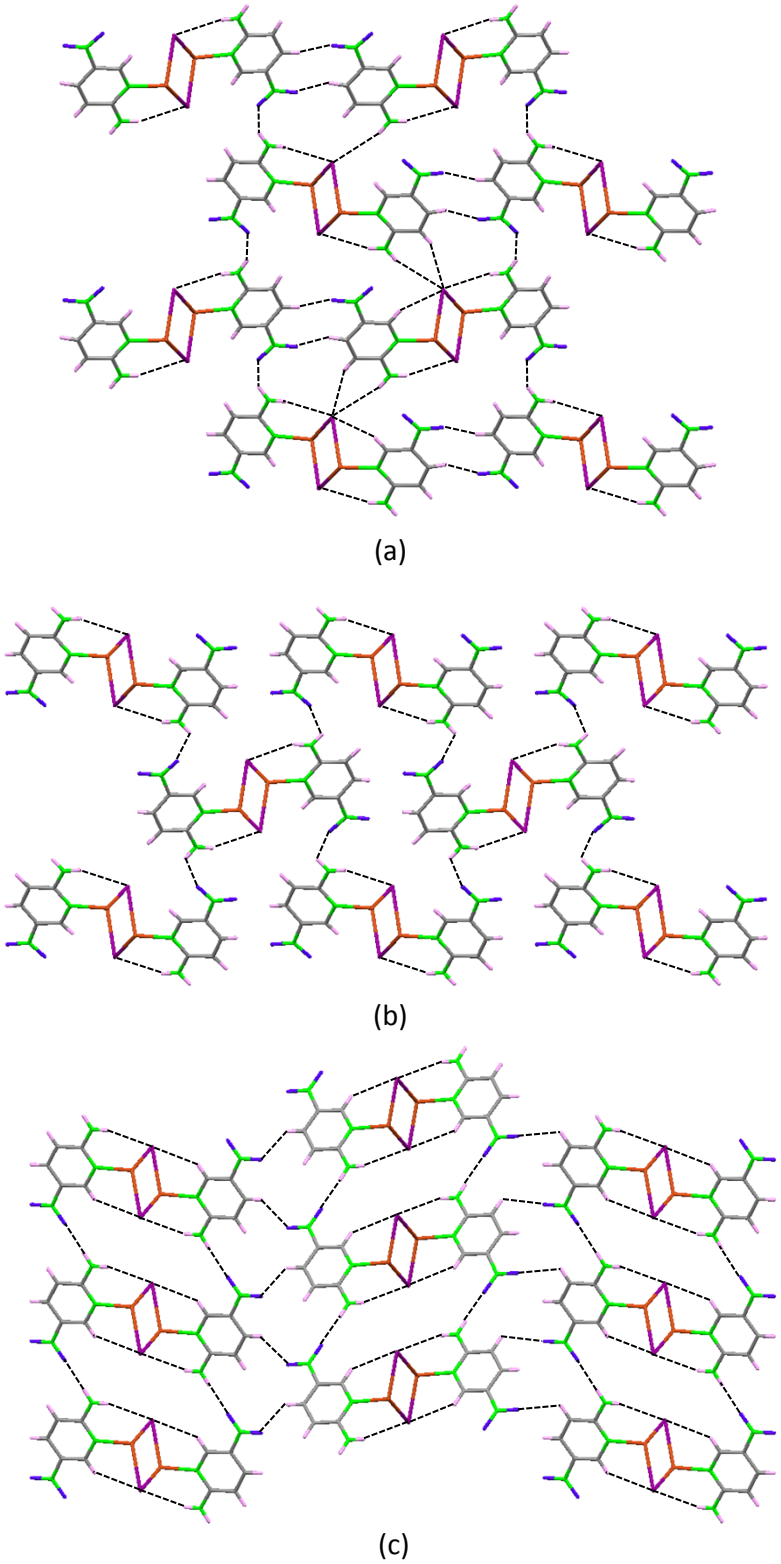

Figure S7. Packing of compounds $\mathbf{1}^{\mathbf{LT}}$ (a), $\mathbf{1}^{\mathbf{RT}}$ (b) and **1a** (c) viewed along the $[Cu(\mu\text{-}I)(C_5H_5N_3O_2)]_n$ chain propagation direction. Dashed lines indicate hydrogen bonding interactions.

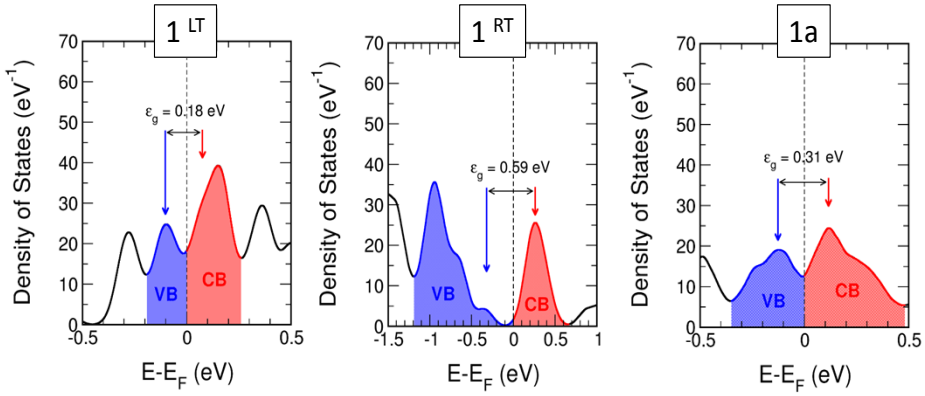

Figure S8. Calculated density of electronic states (in eV^{-1}) for the coordination polymers $\mathbf{1}^{\mathbf{LT}}$, $\mathbf{1}^{\mathbf{RT}}$ and **1a** as a function of the energy, referred to the Fermi level. Each energy level has been broadened with by a Lorentzian profile with a line-width of 0.2 eV, and the valence and conduction bands for all the polymers have been shaded in blue and red, respectively. Transport gap is also indicated in each panel.

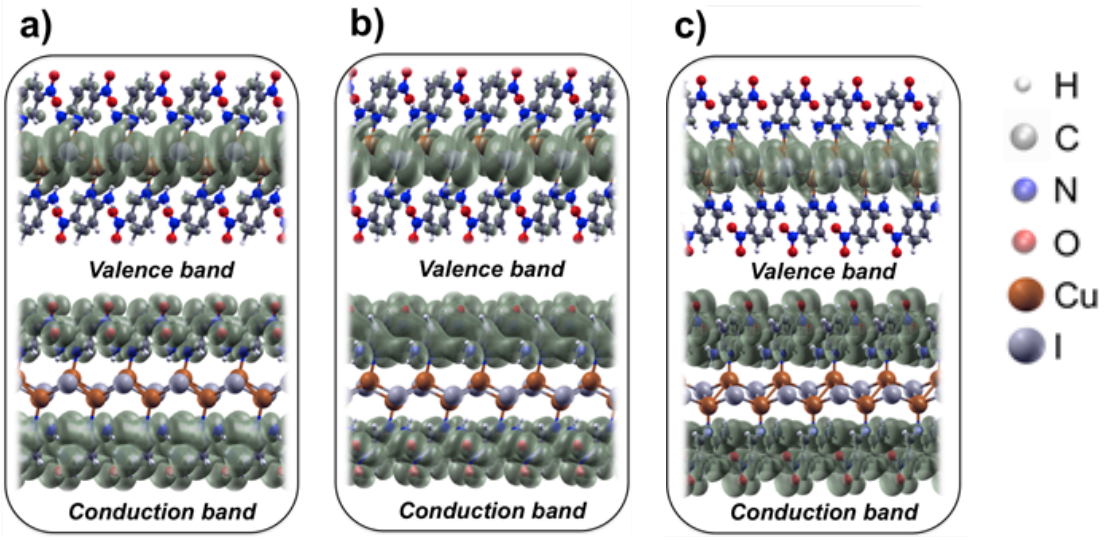

Figure S9. Computed valence (top) and conduction (bottom) band orbital electron isodensities (10^{-4} $e^{-}Å^{-3}$) for the compounds $\mathbf{1}^{\mathbf{LT}}$ (a), $\mathbf{1}^{\mathbf{RT}}$ (b) and **1a** (c).

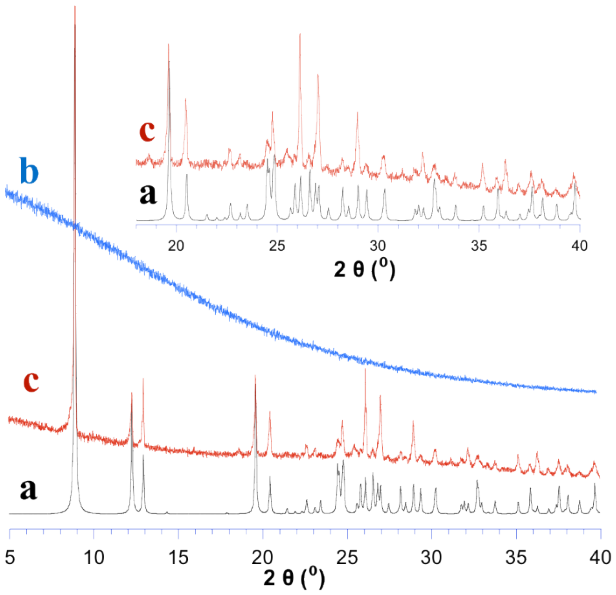

Figure S10. Simulated **(a)** and experimental X-ray powder diffractogram of a polycrystalline sample of compound **1** immersed in acetic glacial acid **(b)** and after removal of the acetic acid **(c)**. Inset shows a zoom of the 18-40º 2θ range.

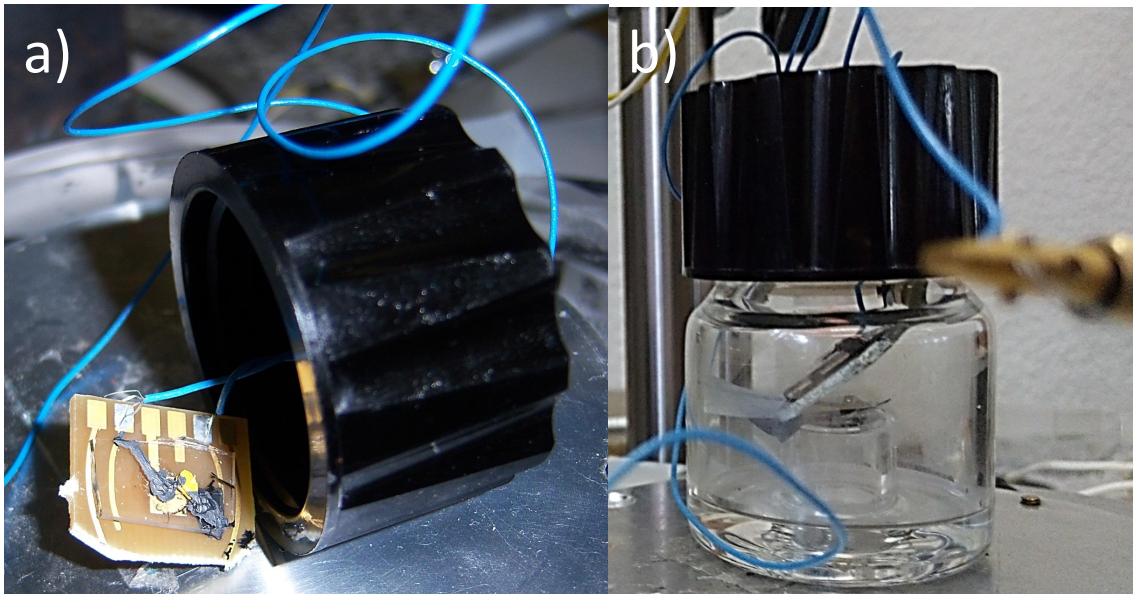

Figure S11. (a) View of the yellow pellet of compound **1** contacted with two electrodes and the cell used to expose the device to vapours of acetic acid (b).

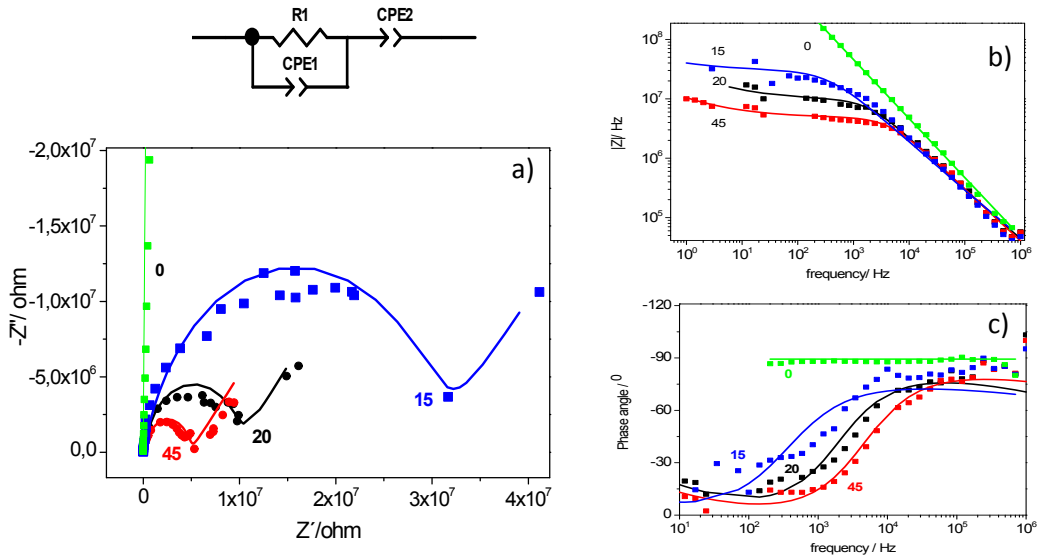

Figure S12. The Nyquist plot (a) and Bode plot (b,c) of compound **1** after different exposed time (0, 45, 15, 20 min.) in HAcO (v). Experimental values (□, •), fitting values (-). The inset in (a) is the equivalent circuit.

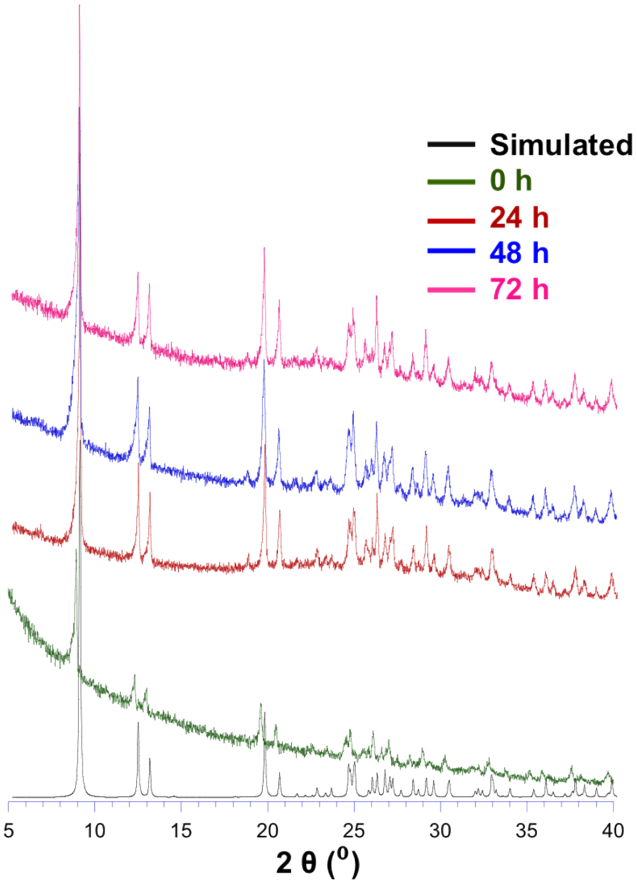

Figure S13. X-ray powder diffractogram in the 5-40º 2θ range of a polycrystalline sample of compound **1** exposed for 24, 48 and 72 h to HAcO vapour.

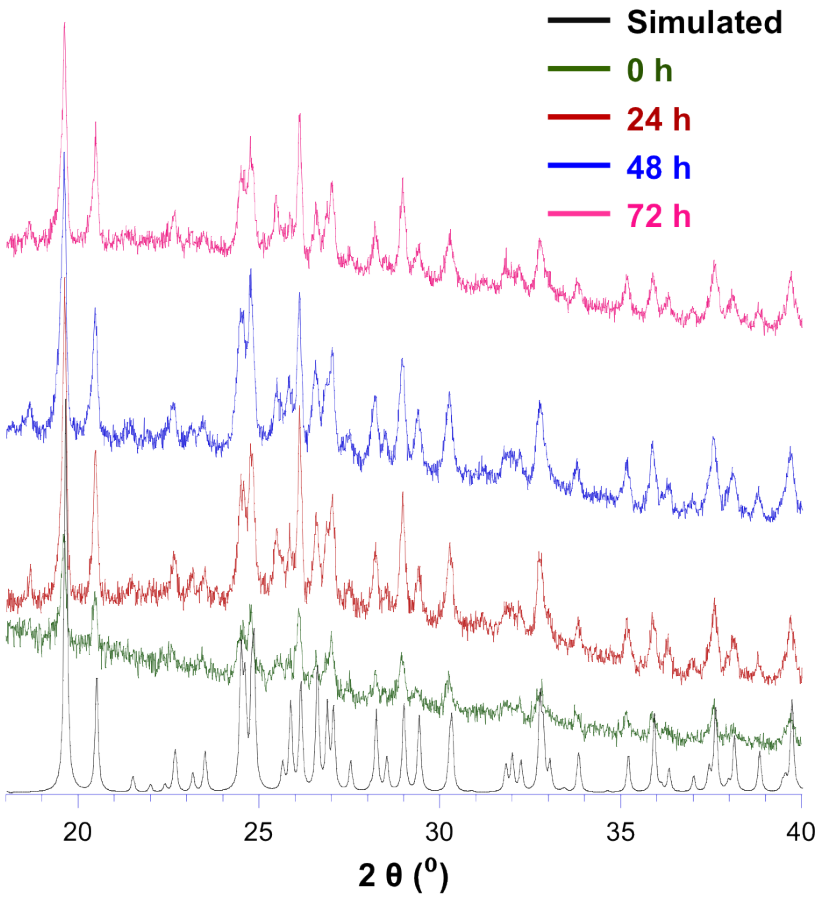

Figure S14. X-ray powder diffractogram in the 18-40º 2θ range of a polycrystalline sample of compound **1** exposed for 24, 48 and 72 h to HAcO vapour.

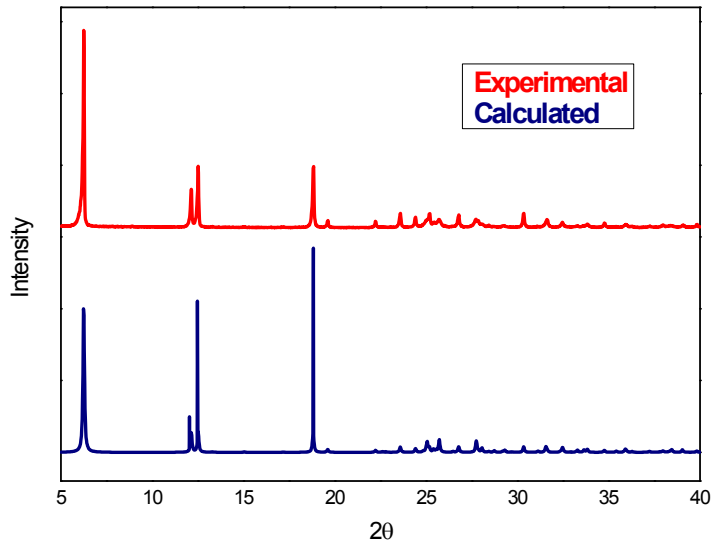

Figure S15. Experimental and calculated X-ray powder diffractogram of **1a.**

REFERENCES

1. L. J. Farrugia, *J. Appl. Cryst.* , 1999, **32**, 837-838.
2. S. D. P. SHELXTL-NT version 6.12, Bruker-Nonius XS, Madison, Wisconsin, USA, 2001.
3. CRYSALISPRO; Oxford Diffraction: Wroclaw, Poland, 2004.
4. G. M. Sheldrick, *SHELXL-97, Program for Crystal Structure Refinement; Universität Göttingen.*, 1997.
5. P. Giannozzi, S. Baroni, N. Bonini, M. Calandra, R. Car, C. Cavazzoni, D. Ceresoli, G. L. Chiarotti, M. Cococcioni, I. Dabo, A. Dal Corso, S. de Gironcoli, S. Fabris, G. Fratesi, R. Gebauer, U. Gerstmann, C. Gougoussis, A. Kokalj, M. Lazzeri, L. Martin-Samos, N. Marzari, F. Mauri, R. Mazzarello, S. Paolini, A. Pasquarello, L. Paulatto, C. Sbraccia, S. Scandolo, G. Sclauzero, A. P. Seitsonen, A. Smogunov, P. Umari and R. M. Wentzcovitch, *J Phys-Condens Mat*, 2009, **21**, 395502.
6. D. Vanderbilt, *Phys Rev B*, 1990, **41**, 7892-7895.
7. J. P. Perdew, K. Burke and M. Ernzerhof, *Phys Rev Lett*, 1996, **77**, 3865-3868.
8. D. J. Chadi and M. L. Cohen, *Phys Rev B*, 1973, **8**, 5747-5753.
9. J. Troyano, J. Perles, P. Amo-Ochoa, J. I. Martinez, F. Zamora and S. Delgado, *Crystengcomm*, 2014, **16**, 8224-8231.